Query Details

Back to Main Page

1. Please confirm if the corresponding author is correctly identified. Amend if necessary.

it is confirmed.

2. Due to the inherent complexities involved in the conversion of DOC/TeX to PDF, please check the equations carefully in the PDF and ensure the data are correctly reproduced.

Ok

3. As References 20 and 41 are same, we have deleted the duplicate reference and renumbered accordingly. Please check and confirm.

Ok

4. Kindly provide the volume number for the reference 2

Ok

Research Article

Validation of the DoseCalcs Monte Carlo code for estimating the ^{18}F *S*-values for ICRP adult and 15-year-old male and female phantoms

Tarik El Ghalbzouri ✉
Email : imttarikk@gmail.com
Affiliationids : Aff1, Correspondingaffiliationid : Aff1

Tarek El Bardouni
Email : tarekelbardouni@gmail.com
Affiliationids : Aff1

Jaafar El Bakkali
Email : bahmedj@gmail.com
Affiliationids : Aff1 Aff2

Hafssa Ziani
Email : hafssaziani94@gmail.com
Affiliationids : Aff1

Abderrahim Doudouh
Email : adoudouh@gmail.com
Affiliationids : Aff1 Aff2 Aff3

Aff1 ERSN Laboratory, Physics Department, Faculty of Sciences, University Abdelmalek Essaadi, Tetouan, Morocco

Aff2 Nuclear Medicine Department, Military Hospital Mohammed V, Rabat, Morocco

Aff3 Faculty of Medicine and Pharmacy, University Mohammed V Souissi, Rabat, Morocco

Received: 5 December 2022 / Revised: 1 March 2023 / Accepted: 2 March 2023

Abstract

Internal radiation exposure using radiopharmaceuticals, as in nuclear medicine procedures, necessitates the estimation of the *S*-value to determine and improve the estimates of absorbed doses in at-risk organs and tissues. The *S* value is defined as the absorbed dose in the target organ per unit of nuclear transformation in the source organ. It is calculated using the specific absorbed fraction, which is an [illegible]tity that connects the deposited energy in the target and emitting source organs. In this study, we applied DoseCalcs, a

new Geant4-based tool, to estimate the *S* values of ^{18}F using nuclear data from ICRP Publication 107. Geometrical data from ICRP Publications 110 and 143 were used to select four models representing male **AQ1** and female phantoms for adults and 15 years old to study the variability in the *S*-values arising from variations in anatomy and initial energy validations, because we used the β mean energy instead of the full beta spectrum. The ^{18}F-released photons and β from 26 source organs were tracked using the Geant4 Livermore package. Accordingly, the *S*-values were calculated for 141 target organs. The results for the adult male and female phantoms were compared with the OpenDose reference data. These results agreed well with OpenDose, the average ratio for self-absorption *S*-values was 1.015, and the average ratios for the cross-irradiation were 1.2 and 1.22 for the AM and AF, respectively. This indicates the accuracy of DoseCalcs for subsequent use in estimating ^{18}F *S*-values using voxelized geometries.

Keywords

DoseCalcs
Geant4
Monte Carlo
Nuclear medicine
S-value
Computational phantom

Supplementary Information

The online version contains supplementary material available at https://doi.org/10.1007/s12194-023-00709-2.

1. Introduction

Nuclear medicine imaging techniques that use radiopharmaceuticals, such as positron emission tomography (PET) and **AQ2** gamma cameras [1, 2], are now widely used in many medical facilities, and their use is continuously expanding. They made an interesting contribution to cancer diagnosis and therapy when they first debuted. Radiation protection is the focus of a large number of scientific researchers worldwide, because these procedures involve radiopharmaceutical products that contain radioactive materials. Scientists are primarily interested in determining ways to protect patients from the biological effects of ionizing radiation while maintaining a high diagnostic image quality [3, 4, 5].

During nuclear fluorodeoxyglucose PET/computed tomography (^{18}F-FDG PET/CT), patients are exposed to two types of irradiation: external and internal. The **AQ3** dose absorbed by the patient from an external radiation source is generated using a CT scanner. This is connected to the PET scanner in areas where significant radiopharmaceutical hyperfixations are likely to occur, resulting in a fusion image with the metabolic image overlaid on the anatomical image. However, internal exposure results **AQ4** from patients receiving an intravenous injection of 2-deoxy-2-^{18}F-fluoro-β-D glucose (^{18}F-FDG), an analog of glucose used for tumor detection and response to cancer therapy [6, 7, 8]. In addition, the tracer accumulation concentration (i.e., the PET image) offers information about tissue metabolic activity, which is known to be higher in cancerous cells than in normal cells. In this study, we focused on the internal components of the radiation-absorbed dose.

The scientific community employs fluorine-18 (^{18}F), a radioisotope of fluorine with a half-life of 109.8 min. It decays 96.73% of the time through positron emission and 3.27% of the time through electron capture. The positron is emitted with a maximum energy of 0.6335 MeV and a mean energy of 0.2498 MeV. Since positrons are unstable in matter, they annihilate an electron in the absorbing medium, producing two annihilation photons traveling in opposite directions. The energy of each annihilation photon corresponds to the rest-mass energy of an electron, that is, 0.511 MeV [9, 10]. ^{18}F is frequently utilized in the molecular imaging of biological and metabolic processes, such as the early detection of various diseases and treatment response assessment using PET [11], because of its short half-life and positron emission.

To minimize the immediate negative effects of ionizing radiation, accurate dose information from the body of a patient injected with ^{18}F-FDG is necessary [12]. These absorbed doses can be calculated accurately in nuclear medicine using Monte Carlo-based dose computations with standard (i.e., non-patient-specific) computational phantoms because of factors such as the heterogeneity of the radioactivity distribution into tissues and organs [13, 14, 15]. Moreover, new treatment planning systems in advanced radiation therapies are attempting to use Monte Carlo simulations for individual patients using CT images for accurate dose estimation [16].

Adult and 15-year-old male and female computational phantoms referenced by the International Commission on Radiological Protection (ICRP) Publications 110 and 143 [17, 18], respectively, and the radionuclide nuclear data and biokinetic data of radiopharmaceuticals enable the prediction of the radiation dose absorbed by each organ as well as several internal dosimetry quantities [19, 20].

For many years, commercial and free softwares, such as MIRDOSE [21] and OLINDA/EXM [22], have been developed to facilitate the computation of patient dosimetry quantities using previously obtained conversion factors in ICRP models. On the other hand, various Monte Carlo tools, such as the general-purpose Monte Carlo N-particle transport code (MCNP) [23], Geant4 [24] application for tomographic emissions (GATE) [25, 26], and DoseCalcs [27], have been developed to calculate the deposited energy or absorbed dose in a given phantom model. Hence, several studies utilizing these codes and others have been conducted. Each of these studies employed a unique set of input data to determine the internal dosimetry quantity for various particles or radionuclides in a given phantom model [28].

This study is primarily aimed at evaluating the newly built code (DoseCalcs) and investigating the variation in ^{18}F *S*-value estimates as a function of patient age and sex by estimating ^{18}F *S*-values using ICRP reference phantoms. In addition, the *S*-value variation was evaluated

when simulating the mean beta energy rather than the entire beta spectrum by comparing the *S*-values calculated by DoseCalcs with OpenDose *S*-values [29].

OpenDose combines 18 international teams to produce and compare dosimetric data using six of the most popular Monte Carlo codes for radiation transport (EGSnrc/EGS++ [30], FLUKA [31], GATE [25], Geant4 [32], MCNP/MCNPX [23], and PENELOPE [33]). OpenDose Monte Carlo simulations were performed with a minimum number of 10^8 mono-energetic photons and electrons, which were emitted isotropically from source regions in the two ICRP 110 adult reference models [17] with a list of 91 energies ranging from 5 keV to 10 MeV. The physics models and simulation parameters were chosen for each team. The secondary particles were generated at an energy threshold of 1 keV. For each combination in a model, the specific absorbed fraction (SAF) value is the mean value of all contributed codes. ~~The physics models and simulation parameters were chosen for each team.~~ Based on the radionuclide decay data presented in ICRP Publication 107 [19], OpenDose S-values were calculated from mono-energetic SAFs. Mono-energetic SAFs were interpolated to calculate the ^{18}F radiation emission (photon of 0.511 MeV and electron of 0.249776 MeV) SAFs.

2. Materials and methods

The Geant4 code (version 11.0) is the framework for the DoseCalcs code, which stands for ”Dosimetry Calculations” [27, 32]. It was developed to provide a simple user platform for scientists with limited experience with Geant4/C++ programming and enable them to perform Monte Carlo calculations using various geometrical approaches, such as voxel-based geometries, geometry description mark-up language (GDML), stereolithography (STL), TEXT, and C++ [34, 35, 36]. Furthermore, the tool includes a simple command interface that directly enters the simulation input data and executes simulations on a computing unit via message-passing interface (MPI) or multithreading (MT) modes [37, 38].

Fig. 1

DoseCalcs code (Based on the Geant4 toolkit) illustrating the executable inputs required to simulate an internal irradiation scenario and produce the desired results

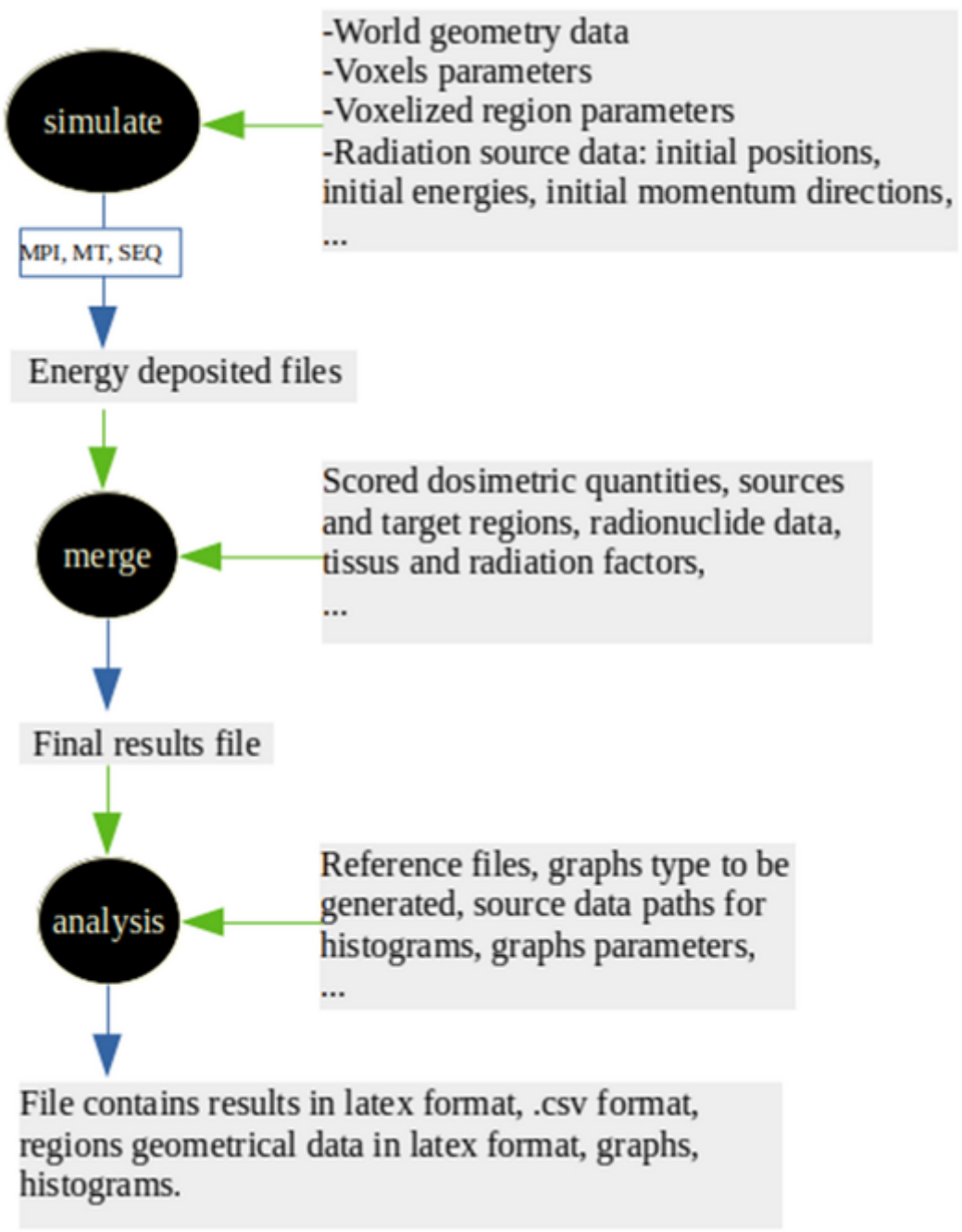

As shown in Fig. 1, DoseCalcs comprises three executables that can be executed on Ubuntu (release 22.~~04~~10) and CentOS (release 7.9) Linux-based systems:

- ***simulate***: It is used to generate primary particle data and simulate or visualize geometry interactively. Three compute modes are available for simulation: sequential (SEQ), MT, and MPI. This executable produces the deposited energy and geometry parameters of all phantom regions for each irradiation source configuration.
- ***merge***: It is used to merge the data files generated by the *simulate* executable and calculate the dosimetry quantities, such as absorbed fraction, ~~specific absorbed fraction~~SAF, *S*-values, absorbed dose, equivalent dose, and effective dose.

Typesetting math: 97%

- ***analysis***: It is an interface for the ROOT analysis system. Based on *merge* generated files, *merge* is used to perform analysis tasks, such as the generation of graphs, histograms, and tables [39].

The input parameters indicated in Fig. 1 were adjusted using a single macro-command file following DoseCalcs user technical notes [27].

2.1. Computational phantoms

In collaboration with the ICRP DOCAL task group, the Helmholtz Zentrum Munchen (German Center for Environmental Health) developed the ICRP adult male and female computational phantoms [17]. ICRP 15-year-old male and female computational phantoms were also developed at the University of Florida (UF) and subsequently at the National Cancer Institute (NCI) [18]. Based on the medical scans of two male and two female individuals, the body height and mass of the adult phantoms and the mass of each organ were adjusted to match the adult males and females specified in ICRP Publication 110.

The voxel sizes for the adult male (Fig. 2 a) and female (Fig. 2 b) were 8 and 4.84 mm in height, respectively, with in-plane resolutions of 2.137 and 1.775 mm and a matrix of 254×127×222 or 7161276 voxels and 299×137×348 or 14255124 voxels [17]. Similarly, for a 15-year-old, the voxel sizes for the male (Fig. 2 c) and female (Fig. 2 d) were 2.832 and 2.828 mm in height, respectively, with in-plane resolutions of 1.25 and 1.2 mm and a matrix of 407×225×586 or 53662950 voxels and 401×236×571 or 54037156 voxels [18]. For brevity, we abbreviated the phantoms as AM, AF, CM, and CF for an adult male, adult female, 15-year-old male, and 15-year-old female computational phantoms, respectively. Each of the 141 segmented organs in these computational phantoms was identified by a unique number in an ASCII file containing ICRP AM, AF, CM, and CF phantom voxel IDs.

Fig. 2

Cross-sectional images in coronal orientation at the middle of the three-dimensional ICRP adult male (**a**), adult female (**b**), 15-year-old male (**c**), and 15-year-old female (**d**) phantoms simulated using DoseCalcs [17, 18]

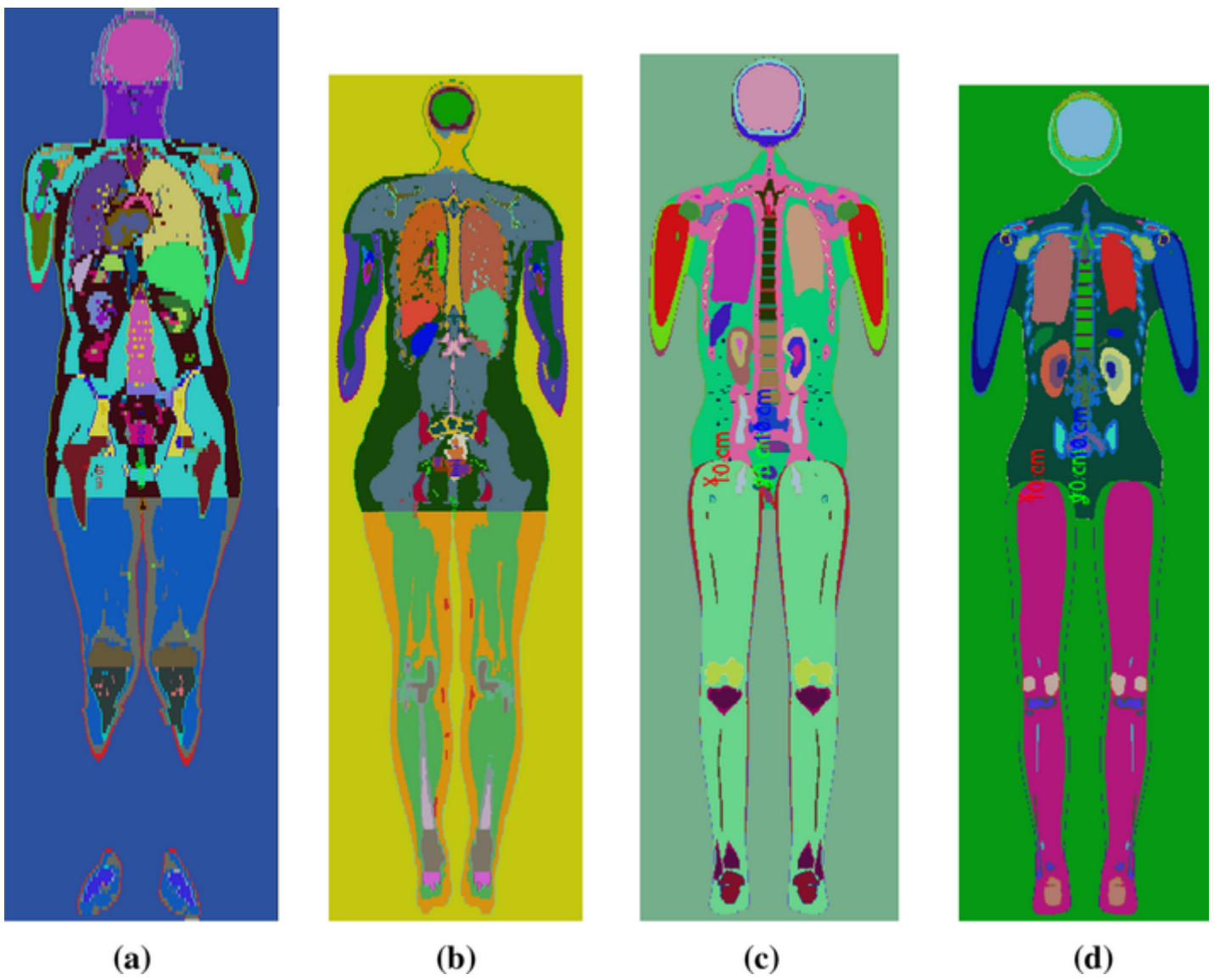

To construct the phantom-region data, the ASCII matrix file of each phantom was used as the DoseCalcs input with a command file. Only the voxel data file path and material command definitions were changed in the DoseCalcs input file to match the anatomy of the simulated phantom in each simulation [17, 18].

2.2. *S*-values' calculations

The ^{18}F *S*-values represent the mean absorbed dose to the target region from the nuclear decay in the source region. According to the MIRD pamphlet 21 [40] and using the nuclear data of ^{18}F provided in [19], the S-values ($S_{r_\mathrm{T}\leftarrow r_\mathrm{S}}\,[\mathrm{Gy}/(\mathrm{Bq}\times\mathrm{s})]$) and the corresponding statistical uncertainty are estimated directly by DoseCalcs as follows:

$$Sr_\mathrm{T} \leftarrow r_\mathrm{S} = \sum_i Y_i \cdot E_i \cdot \frac{\mathrm{ED}_{i,r_\mathrm{T}\leftarrow r_\mathrm{S}}}{\mathrm{EE}_{i,r_\mathrm{S}}} \cdot \frac{1}{M_{r_\mathrm{T}}} \quad (1)$$

$$\sigma(S_{r_T \leftarrow r_S})^2 = \sum_i \left(Y_i E_i \sigma \left(\frac{\mathrm{ED}_{i,r_T \leftarrow r_S}}{\mathrm{EE}_{i,r_S}} \cdot \frac{1}{M_{r_T}} \right) \right)^2; \quad (2)$$

E_i (in Joule) is the individual energy of the i-textitth nuclear transition, Y_i is the number of i-textitth nuclear transitions per nuclear transformation, M_{r_T} (in kilogram) is the mass of the target (r_T) region, and $\mathrm{ED}_{i,r_T \leftarrow r_S}$ (in Joule) is the energy deposited in the target region from the energy emitted by the source (r_S) region, EE_{i,r_S} (in Joule).

2.3. Monte Carlo simulations

Twenty-six organs, including the adrenal left (AdL), adrenal right (AdR), brain, liver, teeth, thymus, spleen, trachea, bronchi, pancreas, heart wall (HeW), esophagus, spinal cord (SpC), rectum wall (ReW), stomach wall (StW), stomach contents (StCs), kidney left cortex (KLC), kidney left pelvis (KLP), kidney left medulla (KLM), kidney right cortex (KRC), kidney right pelvis (KRP), kidney right medulla (KRM), small intestine wall (SIW), urinary bladder wall (UBW), urinary bladder contents (UBCs), and small intestine contents (SICs), were considered to be typical source organs that are characterized by high uptake of ^{18}F. Other tissues and organs were not considered as sources, because the uptake of ^{18}F in those organs is negligible [20, 41].

The Livermore package (*G4Em-LivermorePhysics*) was chosen, because it is suitable for photon and electron transport in medical–physics simulations [42]. The range of secondary particle production for photons, e-, and e+, was fixed at 0.1 mm, and the energy threshold was set to 1 keV.

An electron models the positron with a yield of 96.73% in a Monte Carlo simulation of internal dosimetry, because electrons and positrons lose energy in almost identical ways. The macroscopic cross-section of interactions of the two particles is very close, except for the positron annihilation process, which is modeled by a photon of energy 0.511 MeV with a yield of 193.46% (which is twice the positron yield).

DoseCalcs was used to transport mono-energetic photons of 0.511 MeV and electrons of 0.249776 MeV to model ^{18}F irradiation in the AM, AF, CM, and CF regions. The momentum direction was isotropic, and at the beginning of each event simulation, the three-dimensional uniformly distributed initial positions in the voxels of the source organ were randomly generated. Using the energy deposited by the simulated photons and electrons andas given in Eq. 1, the ^{18}F *S*-values were determined for each target←source.

Subsequently, we used a single input file for each phantom simulation that comprised the voxels and material data, physics, radiation source, run, score, and analysis commands. DoseCalcs was run once per phantom, yielding a total of $4 \times 2 \times 26 = 208$ sub-simulations (four phantoms, photons of 0.511 MeV and electrons of 0.249776 MeV, and 26 source organs). Parallel MPI computing mode was used to run 2×10^8 events on each CPU core. Each of the 208 sub-simulations (combination of phantom, particle energy, and source organ) was modeled automatically by DoseCalcs on the CPU core of an Intel(R) Xeon(R) CPU E5-2620 v3 workstation with 320 CPU cores running at 2.40 GHz. Furthermore, the average CPU time required to run the 208 sub-simulations ranged from 8 h (photons in AM) to 40 h (electrons in AF).

In parallel, Using the same configurations as for ^{18}F simulations, we modeled the radiation emitted from three positron-emitted radionuclides—^{11}C ($T = 20.3$ min, $E_{e-} = 0.385623$ MeV, $Y_{e-} = 99.77$, $E_\gamma = 0.511$ MeV, $Y_\gamma = 199.53$), ^{13}N ($T = 9.97$ min, $E_{e-} = 0.491825$ MeV, $Y_{e-} = 99.80$, $E_\gamma = 0.511$ MeV, $Y_\gamma = 199.61$), and ^{15}O ($T = 2.1$ min, $E_{e-} = 0.735422$ MeV, $Y_{e-} = 99.90$, $E_\gamma = 0.511$ MeV, $Y_\gamma = 199.80$)—in the AM phantom in parallel to verify the capability of DoseCalcs for *S*-values' prediction.

3. Results and discussion

Because of the large number of target←source combinations resulting in the simulations, the DoseCalcs-discussed results for the simulation of internal irradiation by ^{18}F in AM, AF, CM, and CF are presented in Tables 1 and 2 and Figs. 3 and 4. This shows that the self-absorption *S*-values (S-S), source organ, and target organ are the same, and the cross-irradiation *S*-values (C-S), source organs, and target organs are different, along with the corresponding relative standard deviation in percent (RSD%) in the AM, AF, CM, and CF phantoms for specific source regions and target←source combinations. In addition, the complete dataset of all the simulated source regions and the resulting combinations are provided in a numerical format in the supplementary data.

In this study, we validated the DoseCalcs-derived S-values by comparing the results with the OpenDose database, which provides S-values for two models (ICRP adult males and females), 141 sources, 172 targets, and 1252 radioisotopes [29].

Table 1

Self-absorption *S*-values (mGy/(MBq s)) of ^{18}F for each source region calculated in the simulated geometries by DoseCalcs and compared to the OpenDose reference data [29]

Source Region	Method	Phantoms			
		Adult Female	Adult Male	Female 15 years	Male 15 years
[a]Ratio					
[b]Relative Standard Deviation (%)					

Source Region	Method	Phantoms			
		Adult Female	Adult Male	Female 15 years	Male 15 years
AdL	DoseCalcs	7.1645e−03	5.4742e−03	8.7397e−03	7.6017e−03
	OpenDose (R)[a]	7.0504e−03 (1.02)	5.4518e−03 (1.00)	N/A (–)	N/A (–)
	RSD(%)[b]	1.2302e−04	1.4548e−04	1.3028e−04	1.2931e−04
AdR	DoseCalcs	5.6460e−03	5.6506e−03	9.0408e−03	8.6374e−03
	OpenDose (R)[a]	5.5487e−03 (1.02)	5.5047e−03 (1.03)	N/A (–)	N/A (–)
	RSD(%)[b]	1.2133e−04	1.4361e−04	1.3015e−04	1.3090e−04
Brain	DoseCalcs	4.9157e−05	4.4702e−05	4.9356e−05	4.5540e−05
	OpenDose (R)[a]	4.8723e−05 (1.01)	4.4319e−05 (1.01)	N/A (–)	N/A (–)
	RSD(%)[b]	4.9653e−05	5.1278e−05	4.2003e−05	4.4000e−05
Bronchi	DoseCalcs	4.2205e−03	5.6557e−04	6.0036e−03	5.5459e−03
	OpenDose (R)[a]	4.0395e−03 (1.04)	5.4210e−04 (1.04)	N/A (–)	N/A (–)
	RSD(%)[b]	1.7719e−04	1.5531e−04	1.1566e−04	1.2316e−04
HeW	DoseCalcs	1.8076e−04	1.3911e−04	2.0433e−04	1.9385e−04
	OpenDose (R)[a]	1.7797e−04 (1.02)	1.3701e−04 (1.02)	N/A (–)	N/A (–)
	RSD(%)[b]	8.4205e−05	6.1170e−05	7.2269e−05	7.8044e−05
KLC	DoseCalcs	4.3823e−04	4.2644e−04	5.1558e−04	4.9361e−04
	OpenDose (R)[a]	4.3297e−04 (1.01)	4.2149e−04 (1.01)	N/A (–)	N/A (–)
	RSD(%)[b]	8.3454e−05	8.8991e−05	7.2702e−05	7.7657e−05
KLM	DoseCalcs	1.1434e−03	1.1311e−03	1.3865e−03	1.3251e−03
	OpenDose (R)[a]	1.1224e−03 (1.02)	1.1142e−03 (1.02)	N/A (–)	N/A (–)
	RSD(%)[b]	9.9122e−05	1.0307e−04	8.1286e−05	8.7460e−05
KLP	DoseCalcs	5.3139e−03	5.2896e−03	6.5320e−03	6.3429e−03
	OpenDose (R)[a]	5.1843e−03 (1.02)	5.1848e−03 (1.02)	N/A (–)	N/A (–)
	RSD(%)[b]	1.3182e−04	1.3567e−04	1.0002e−04	1.0573e−04
KRC	DoseCalcs	5.1481e−04	4.1887e−04	5.1482e−04	4.9215e−04
	OpenDose (R)[a]	5.0813e−04 (1.01)	4.1413e−04 (1.01)	N/A (–)	N/A (–)
	RSD(%)[b]	8.6079e−05	8.7184e−05	7.3288e−05	7.8754e−05
KRM	DoseCalcs	1.3475e−03	1.1075e−03	1.3799e−03	1.3235e−03
	OpenDose (R)[a]	1.3216e−03 (1.02)	1.0918e−03 (1.01)	N/A (–)	N/A (–)
	RSD(%)[b]	1.0261e−04	1.0182e−04	8.1748e−05	8.7408e−05
KRP	DoseCalcs	6.3859e−03	5.1480e−03	6.6142e−03	6.3106e−03
	OpenDose (R)[a]	6.2485e−03 (1.02)	5.0487e−03 (1.02)	N/A (–)	N/A (–)
	RSD(%)[b]	1.3202e−04	1.3514e−04	1.0029e−04	1.0586e−04
Liver	DoseCalcs	4.4475e−05	3.6142e−05	4.7817e−05	4.8022e−05
	OpenDose (R)[a]	4.4145e−05 (1.01)	3.5908e−05 (1.01)	N/A (–)	N/A (–)
	RSD(%)[b]	5.0949e−05	5.0727e−05	4.3582e−05	4.5944e−05
Esophagus	DoseCalcs	1.1762e−03	1.0337e−03	1.3741e−03	1.3764e−03
	OpenDose (R)[a]	1.1563e−03 (1.02)	1.0170e−03 (1.02)	N/A (–)	N/A (–)
	RSD(%)[b]	1.1962e−04	1.2412e−04	1.0423e−04	1.1114e−04
Pancreas	DoseCalcs	3.9556e−04	3.5133e−04	4.6702e−04	4.2994e−04
	OpenDose (R)[a]	3.9266e−04 (1.01)	3.4926e−04 (1.01)	N/A (–)	N/A (–)
	RSD(%)[b]	7.9175e−05	7.7294e−05	6.7787e−05	7.1557e−05

[a]Ratio

[b]Relative Standard Deviation (%)

Source Region	Method	Phantoms			
		Adult Female	Adult Male	Female 15 years	Male 15 years
ReW	DoseCalcs	1.7701e−03	1.4878e−03	1.8997e−02	6.2898e−03
	OpenDose (R)[a]	1.7529e−03 (1.01)	1.4743e−03 (1.01)	N/A (–)	N/A (–)
	RSD(%)[b]	9.5313e−05	9.8382e−05	1.3079e−04	1.1649e−04
SICs	DoseCalcs	1.6012e−04	1.3136e−04	1.5664e−04	1.4694e−04
	OpenDose (R)[a]	1.5791e−04 (1.01)	1.2961e−04 (1.01)	N/A (–)	N/A (–)
	RSD(%)[b]	8.7512e−05	8.5377e−05	5.8652e−05	6.7857e−05
SIW	DoseCalcs	7.6834e−05	6.9146e−05	8.4004e−05	8.3993e−05
	OpenDose (R)[a]	7.5503e−05 (1.02)	6.7717e−05 (1.02)	N/A (–)	N/A (–)
	RSD(%)[b]	7.8409e−05	8.5882e−05	7.0806e−05	7.6534e−05
SpC	DoseCalcs	2.0902e−03	1.0962e−03	7.2834e−04	8.5836e−04
	OpenDose (R)[a]	2.0359e−03 (1.03)	1.0743e−03 (1.02)	N/A (–)	N/A (–)
	RSD(%)[b]	1.4856e−04	1.3859e−04	1.0111e−04	1.0845e−04
Spleen	DoseCalcs	3.7248e−04	3.3096e−04	3.7677e−04	3.7023e−04
	OpenDose (R)[a]	3.6997e−04 (1.01)	3.2899e−04 (1.01)	N/A (–)	N/A (–)
	RSD(%)[b]	7.5776e−05	7.5735e−05	6.4199e−05	7.0037e−05
StCs	DoseCalcs	2.1925e−04	1.9902e−04	2.5534e−04	2.5569e−04
	OpenDose (R)[a]	2.1787e−04 (1.01)	1.9766e−04 (1.01)	N/A (–)	N/A (–)
	RSD(%)[b]	6.9663e−05	7.4986e−05	5.6726e−05	6.1889e−05
StW	DoseCalcs	3.0464e−04	2.8330e−04	3.5212e−04	3.3661e−04
	OpenDose (R)[a]	2.9849e−04 (1.02)	2.7758e−04 (1.02)	N/A (–)	N/A (–)
	RSD(%)[b]	9.7785e−05	1.0430e−04	8.6658e−05	1.0555e−04
Teeth	DoseCalcs	1.1949e−03	9.5923e−04	1.3422e−03	1.0742e−03
	OpenDose (R)[a]	1.1930e−03 (1.00)	9.5839e−04 (1.00)	N/A (–)	N/A (–)
	RSD(%)[b]	9.2220e−05	9.5616e−05	8.6742e−05	8.5111e−05
Thymus	DoseCalcs	2.1126e−03	1.7294e−03	1.4854e−03	1.2856e−03
	OpenDose (R)[a]	2.0799e−03 (1.02)	1.7086e−03 (1.01)	N/A (–)	N/A (–)
	RSD(%)[b]	1.0752e−04	1.0656e−04	7.9122e−05	8.0272e−05
Trachea	DoseCalcs	4.6801e−03	3.7966e−03	6.5667e−03	5.5353e−03
	OpenDose (R)[a]	4.5091e−03 (1.04)	3.6722e−03 (1.03)	N/A (–)	N/A (–)
	RSD(%)[b]	1.7209e−04	1.6925e−04	1.3854e−04	1.2263e−04
UBCs	DoseCalcs	2.5890e−04	2.6169e−04	3.7480e−04	3.3245e−04
	OpenDose (R)[a]	2.5733e−04 (1.01)	2.6033e−04 (1.01)	N/A (–)	N/A (–)
	RSD(%)[b]	6.6733e−05	6.8974e−05	5.8898e−05	6.1016e−05
UBW	DoseCalcs	9.5845e−04	7.9299e−04	1.0943e−03	9.6591e−04
	OpenDose (R)[a]	9.2112e−04 (1.04)	7.6871e−04 (1.03)	N/A (–)	N/A (–)
	RSD(%)[b]	1.3278e−04	1.2633e−04	1.1209e−04	1.1686e−04
[a]Ratio					
[b]Relative Standard Deviation (%)					

Table 2

Cross-irradiation *S*-values (mGy/(MBq s)) of ^{18}F for each source–target combination calculated in the simulated geometries using DoseCalcs and compared to the OpenDose reference data [29]

Target←source	Method	Phantoms			
		Adult Female	Adult Male	Female 15 years	Male 15 years
[a] Ratio					
[b] Relative Standard Deviation (%)					

Target←source	Method	Phantoms			
		Adult Female	Adult Male	Female 15 years	Male 15 years
Liver←Brain	DoseCalcs	5.5093e−08	4.4028e−08	6.6676e−08	4.6727e−08
	OpenDose (R)[a]	4.5538e−08 (1.21)	3.7690e−08 (1.17)	N/A (–)	N/A (–)
	RSD(%)[b]	2.2481e−02	3.0651e−02	2.7174e−02	3.6818e−02
Spleen←Brain	DoseCalcs	5.6962e−08	4.7552e−08	6.1698e−08	4.5688e−08
	OpenDose (R)[a]	4.5390e−08 (1.25)	3.7118e−08 (1.28)	N/A (–)	N/A (–)
	RSD(%)[b]	1.1773e−01	1.2940e−01	9.3987e−02	1.0419e−01
Pancreas←Brain	DoseCalcs	2.5151e−08	2.3908e−08	3.6719e−08	2.5854e−08
	OpenDose (R)[a]	2.0719e−08 (1.21)	1.8572e−08 (1.29)	N/A (–)	N/A (–)
	RSD(%)[b]	1.5365e−01	1.5650e−01	1.7623e−01	1.2445e−01
HeW←Brain	DoseCalcs	1.5075e−07	1.0532e−07	1.6889e−07	1.4625e−07
	OpenDose (R)[a]	1.1700e−07 (1.29)	7.7487e−08 (1.36)	N/A (–)	N/A (–)
	RSD(%)[b]	3.3112e−02	3.2807e−02	3.0078e−02	3.4215e−02
SIW←Brain	DoseCalcs	1.0384e−08	9.3152e−09	1.5862e−08	1.1293e−08
	OpenDose (R)[a]	8.3460e−09 (1.24)	7.2182e−09 (1.29)	N/A (–)	N/A (–)
	RSD(%)[b]	9.9085e−02	1.5006e−01	1.1251e−01	1.2479e−01
UBW←Brain	DoseCalcs	1.5891e−09	1.4579e−09	3.1284e−09	2.4230e−09
	OpenDose (R)[a]	1.3152e−09 (1.21)	1.0044e−09 (1.45)	N/A (–)	N/A (–)
	RSD(%)[b]	3.2936e−02	2.9912e−02	2.2135e−02	2.5302e−02
StW←Brain	DoseCalcs	3.9560e−08	3.5587e−08	4.9643e−08	3.8170e−08
	OpenDose (R)[a]	3.2007e−08 (1.24)	2.8248e−08 (1.26)	N/A (–)	N/A (–)
	RSD(%)[b]	1.0945e−01	1.1154e−01	1.3815e−01	1.4772e−01
Brain←HeW	DoseCalcs	1.4624e−07	1.0229e−07	1.6234e−07	1.3899e−07
	OpenDose (R)[a]	1.1350e−07 (1.29)	7.4177e−08 (1.38)	N/A (–)	N/A (–)
	RSD(%)[b]	1.4544e−02	1.7088e−02	1.3628e−02	1.4472e−02
Liver←HeW	DoseCalcs	2.9780e−06	2.5939e−06	3.3629e−06	2.2972e−06
	OpenDose (R)[a]	2.8617e−06 (1.04)	2.5020e−06 (1.04)	N/A (–)	N/A (–)
	RSD(%)[b]	3.3905e−04	7.3264e−04	4.3412e−04	5.3273e−04
Spleen←HeW	DoseCalcs	3.1645e−06	2.7927e−06	1.7747e−06	1.3377e−06
	OpenDose (R)[a]	3.0319e−06 (1.04)	2.6967e−06 (1.04)	N/A (–)	N/A (–)
	RSD(%)[b]	4.5791e−03	4.3635e−03	5.9400e−03	7.0066e−03
Pancreas←HeW	DoseCalcs	1.2963e−06	1.7733e−06	1.2866e−06	1.0097e−06
	OpenDose (R)[a]	1.1986e−06 (1.08)	1.7033e−06 (1.04)	N/A (–)	N/A (–)
	RSD(%)[b]	9.4798e−03	6.5765e−03	8.8259e−03	9.3054e−03
HeW←HeW	DoseCalcs	1.8076e−04	1.3911e−04	2.0433e−04	1.9385e−04
	OpenDose (R)[a]	1.7797e−04 (1.02)	1.3701e−04 (1.02)	N/A (–)	N/A (–)
	RSD(%)[b]	8.4205e−05	6.1170e−05	7.2269e−05	7.8044e−05
SIW←HeW	DoseCalcs	4.4746e−07	5.4390e−07	4.5715e−07	3.4161e−07
	OpenDose (R)[a]	3.9523e−07 (1.13)	5.0060e−07 (1.09)	N/A (–)	N/A (–)
	RSD(%)[b]	7.9051e−03	6.2937e−03	7.9344e−03	9.6806e−03
UBW←HeW	DoseCalcs	4.8169e−08	5.4170e−08	7.7484e−08	7.0310e−08
	OpenDose (R)[a]	3.5980e−08 (1.34)	4.2152e−08 (1.29)	N/A (–)	N/A (–)
	RSD(%)[b]	3.9929e−01	1.4205e−01	1.0396e−01	1.4153e−01
[a] Ratio					
[b] Relative Standard Deviation (%)					

Target←source	Method	Phantoms			
		Adult Female	Adult Male	Female 15 years	Male 15 years
StW←HeW	DoseCalcs	3.6179e−06	5.0440e−06	3.0225e−06	2.2754e−06
	OpenDose (R)[a]	3.5026e−06 (1.03)	4.9698e−06 (1.01)	N/A (–)	N/A (–)
	RSD(%)[b]	6.7007e−04	4.7472e−04	4.2698e−03	4.9752e−03
Brain←Liver	DoseCalcs	5.3157e−08	4.2968e−08	6.3691e−08	4.4289e−08
	OpenDose (R)[a]	4.3888e−08 (1.21)	3.5822e−08 (1.20)	N/A (–)	N/A (–)
	RSD(%)[b]	3.0669e−02	2.9715e−02	2.6313e−02	3.5179e−02
Liver←Liver	DoseCalcs	4.4475e−05	3.6142e−05	4.7817e−05	4.8022e−05
	OpenDose (R)[a]	4.4145e−05 (1.01)	3.5908e−05 (1.01)	N/A (–)	N/A (–)
	RSD(%)[b]	5.0949e−05	5.0727e−05	4.3582e−05	4.5944e−05
Spleen←Liver	DoseCalcs	2.0554e−06	1.1266e−06	1.4572e−06	1.1418e−06
	OpenDose (R)[a]	1.9462e−06 (1.06)	1.0612e−06 (1.06)	N/A (–)	N/A (–)
	RSD(%)[b]	6.2463e−03	8.7243e−03	7.0960e−03	8.0067e−03
Pancreas←Liver	DoseCalcs	5.5910e−06	5.7960e−06	3.1892e−06	2.2247e−06
	OpenDose (R)[a]	5.4468e−06 (1.03)	5.7007e−06 (1.02)	N/A (–)	N/A (–)
	RSD(%)[b]	1.1406e−03	1.0642e−03	4.6411e−03	5.7093e−03
HeW←Liver	DoseCalcs	2.9783e−06	2.5942e−06	3.3625e−06	2.2935e−06
	OpenDose (R)[a]	2.8633e−06 (1.04)	2.5037e−06 (1.04)	N/A (–)	N/A (–)
	RSD(%)[b]	7.9942e−04	1.7256e−03	1.0844e−03	1.2923e−03
SIW←Liver	DoseCalcs	1.5819e−06	1.1561e−06	1.9781e−06	1.5418e−06
	OpenDose (R)[a]	1.4989e−06 (1.06)	1.0862e−06 (1.06)	N/A (–)	N/A (–)
	RSD(%)[b]	5.9577e−04	1.7404e−03	2.8101e−03	3.4783e−03
UBW←Liver	DoseCalcs	1.4696e−07	1.3999e−07	2.3204e−07	2.3394e−07
	OpenDose (R)[a]	1.1485e−07 (1.28)	1.1221e−07 (1.25)	N/A (–)	N/A (–)
	RSD(%)[b]	7.2223e−02	7.6973e−02	7.4699e−02	5.6320e−02
StW←Liver	DoseCalcs	4.6562e−06	3.6130e−06	3.7889e−06	3.2872e−06
	OpenDose (R)[a]	4.5686e−06 (1.02)	3.5402e−06 (1.02)	N/A (–)	N/A (–)
	RSD(%)[b]	5.1886e−04	8.0798e−04	3.9032e−03	4.4449e−03
Brain←SICs	DoseCalcs	1.1813e−08	1.4056e−08	1.5269e−08	1.0640e−08
	OpenDose (R)[a]	9.3609e−09 (1.26)	1.0350e−08 (1.36)	N/A (–)	N/A (–)
	RSD(%)[b]	8.1733e−02	1.0000e−01	7.7139e−02	9.4677e−02
Liver←SICs	DoseCalcs	1.8324e−06	1.8293e−06	1.9577e−06	1.5171e−06
	OpenDose (R)[a]	1.7333e−06 (1.06)	1.7510e−06 (1.04)	N/A (–)	N/A (–)
	RSD(%)[b]	7.3526e−04	9.9653e−04	1.8147e−03	2.1880e−03
Spleen←SICs	DoseCalcs	2.0101e−06	2.5865e−06	1.1283e−06	9.7271e−07
	OpenDose (R)[a]	1.9078e−06 (1.05)	2.4890e−06 (1.04)	N/A (–)	N/A (–)
	RSD(%)[b]	5.7298e−03	4.5042e−03	8.1220e−03	8.9989e−03
Pancreas←SICs	DoseCalcs	1.0177e−05	9.7458e−06	4.1838e−06	4.1970e−06
	OpenDose (R)[a]	1.0150e−05 (1.00)	9.7230e−06 (1.00)	N/A (–)	N/A (–)
	RSD(%)[b]	3.8922e−04	3.9794e−04	3.8013e−03	3.6184e−03
HeW←SICs	DoseCalcs	5.5987e−07	9.6829e−07	4.5461e−07	3.3955e−07
	OpenDose (R)[a]	5.0109e−07 (1.12)	9.0962e−07 (1.06)	N/A (–)	N/A (–)
	RSD(%)[b]	9.8390e−03	6.2860e−03	1.1370e−02	1.4957e−02

[a] Ratio

[b] Relative Standard Deviation (%)

Typesetting math: 97%

Target←source	Method	Phantoms			
		Adult Female	Adult Male	Female 15 years	Male 15 years
SIW←SICs	DoseCalcs	1.4248e−05	1.1707e−05	1.7455e−05	1.6933e−05
	OpenDose (R)[a]	1.4902e−05 (0.96)	1.2284e−05 (0.95)	N/A (–)	N/A (–)
	RSD(%)[b]	1.2104e−04	1.3497e−04	1.0560e−04	1.1386e−04
UBW←SICs	DoseCalcs	4.1361e−06	1.1427e−06	2.2968e−06	2.8619e−06
	OpenDose (R)[a]	4.0338e−06 (1.03)	1.0781e−06 (1.06)	N/A (–)	N/A (–)
	RSD(%)[b]	1.4770e−03	2.8249e−03	1.0249e−02	8.8054e−03
StW←SICs	DoseCalcs	5.5371e−06	4.7504e−06	2.3721e−06	2.1986e−06
	OpenDose (R)[a]	5.4121e−06 (1.02)	4.6388e−06 (1.02)	N/A (–)	N/A (–)
	RSD(%)[b]	7.1138e−04	1.1134e−03	1.4267e−03	1.9928e−03
Brain←StCs	DoseCalcs	4.3745e−08	3.5679e−08	4.0425e−08	2.6770e−08
	OpenDose (R)[a]	3.4672e−08 (1.26)	2.6598e−08 (1.34)	N/A (–)	N/A (–)
	RSD(%)[b]	3.4706e−02	4.0009e−02	3.5029e−02	5.7919e−02
Liver←StCs	DoseCalcs	4.3379e−06	3.0627e−06	3.7351e−06	2.9804e−06
	OpenDose (R)[a]	4.2078e−06 (1.03)	2.9788e−06 (1.03)	N/A (–)	N/A (–)
	RSD(%)[b]	4.3220e−04	4.0736e−04	1.2474e−03	1.4686e−03
Spleen←StCs	DoseCalcs	1.3561e−05	6.5144e−06	6.6965e−06	4.0701e−06
	OpenDose (R)[a]	1.3342e−05 (1.02)	6.3703e−06 (1.02)	N/A (–)	N/A (–)
	RSD(%)[b]	1.8259e−03	2.6348e−03	2.7093e−03	3.4972e−03
Pancreas←StCs	DoseCalcs	9.8091e−06	6.8079e−06	1.2008e−05	1.3475e−05
	OpenDose (R)[a]	9.6606e−06 (1.02)	6.7243e−06 (1.01)	N/A (–)	N/A (–)
	RSD(%)[b]	1.2771e−03	1.3798e−03	2.2676e−03	2.1024e−03
HeW←StCs	DoseCalcs	4.6944e−06	5.8211e−06	2.1600e−06	1.2710e−06
	OpenDose (R)[a]	4.5598e−06 (1.03)	5.7527e−06 (1.01)	N/A (–)	N/A (–)
	RSD(%)[b]	5.5077e−04	3.3593e−04	3.9154e−03	5.2253e−03
SIW←StCs	DoseCalcs	2.9765e−06	2.3389e−06	2.8882e−06	3.1200e−06
	OpenDose (R)[a]	2.8749e−06 (1.04)	2.2600e−06 (1.03)	N/A (–)	N/A (–)
	RSD(%)[b]	5.8574e−04	8.2875e−04	1.1773e−03	1.0356e−03
UBW←StCs	DoseCalcs	1.6384e−07	1.4405e−07	3.3711e−07	4.2227e−07
	OpenDose (R)[a]	1.2748e−07 (1.29)	1.1597e−07 (1.24)	N/A (–)	N/A (–)
	RSD(%)[b]	7.8267e−02	6.3607e−02	4.4226e−02	3.4643e−02
StW←StCs	DoseCalcs	3.1463e−05	2.9157e−05	3.1973e−05	2.5225e−05
	OpenDose (R)[a]	3.2726e−05 (0.96)	3.0316e−05 (0.96)	N/A (–)	N/A (–)
	RSD(%)[b]	1.6712e−04	1.7597e−04	1.5536e−04	1.7775e−04
Brain←UBCs	DoseCalcs	1.7348e−09	1.3790e−09	3.1150e−09	2.3116e−09
	OpenDose (R)[a]	1.2316e−09 (1.41)	9.9007e−10 (1.39)	N/A (–)	N/A (–)
	RSD(%)[b]	1.4794e−01	5.8810e−03	2.0714e−01	1.2404e−01
Liver←UBCs	DoseCalcs	1.5885e−07	1.4821e−07	2.4031e−07	2.3288e−07
	OpenDose (R)[a]	1.2419e−07 (1.28)	1.2155e−07 (1.22)	N/A (–)	N/A (–)
	RSD(%)[b]	1.2456e−02	1.1073e−02	9.0917e−03	8.9722e−03
Spleen←UBCs	DoseCalcs	1.2239e−07	1.1047e−07	2.0567e−07	1.9762e−07
	OpenDose (R)[a]	9.6478e−08 (1.27)	8.7997e−08 (1.26)	N/A (–)	N/A (–)
	RSD(%)[b]	6.1310e−02	5.2667e−02	3.4273e−02	3.5125e−02

[a] Ratio

[b] Relative Standard Deviation (%)

Target←source	Method	Phantoms			
		Adult Female	Adult Male	Female 15 years	Male 15 years
Pancreas←UBCs	DoseCalcs	3.4971e−07	2.9081e−07	4.2880e−07	5.0413e−07
	OpenDose (R)[a]	2.9815e−07 (1.17)	2.5518e−07 (1.14)	N/A (–)	N/A (–)
	RSD(%)[b]	2.6553e−02	2.7860e−02	2.0688e−02	1.8726e−02
HeW←UBCs	DoseCalcs	5.1968e−08	5.6677e−08	8.0531e−08	7.0082e−08
	OpenDose (R)[a]	3.7751e−08 (1.38)	4.5165e−08 (1.25)	N/A (–)	N/A (–)
	RSD(%)[b]	5.1957e−02	4.9542e−02	4.8181e−02	5.7055e−02
SIW←UBCs	DoseCalcs	4.8223e−06	3.1553e−06	2.4157e−06	2.6931e−06
	OpenDose (R)[a]	4.7131e−06 (1.02)	3.0601e−06 (1.03)	N/A (–)	N/A (–)
	RSD(%)[b]	3.7352e−04	5.9642e−04	2.4031e−03	2.3437e−03
UBW←UBCs	DoseCalcs	4.6951e−05	4.5059e−05	6.3932e−05	5.7194e−05
	OpenDose (R)[a]	4.9969e−05 (0.94)	4.7507e−05 (0.95)	N/A (–)	N/A (–)
	RSD(%)[b]	2.6540e−04	2.5216e−04	2.0993e−04	2.1738e−04
StW←UBCs	DoseCalcs	2.1971e−07	1.6457e−07	3.0506e−07	3.2025e−07
	OpenDose (R)[a]	1.7798e−07 (1.23)	1.3617e−07 (1.21)	N/A (–)	N/A (–)
	RSD(%)[b]	3.0731e−02	3.2957e−02	2.3185e−02	2.5245e−02

[a] Ratio

[b] Relative Standard Deviation (%)

Table 1 and Fig. 3 show the S-S in the regions that were simulated as sources of ^{18}F. A large part of the energy of 0.511 MeV photons is deposited outside the source organs. However, the electrons deposit the large part of their energies in the source organs, resulting in the absorbed fraction being unity. Hence, the S-values are inversely proportional to organ mass. This makes the S-values of the younger phantoms larger than those of the older phantoms.

Overall, the calculated S-Ss from the adult phantoms were much lower than those from the 15-year-old phantoms. However, the S-Ss in the SpC and thymus were much higher in the adult phantoms, because the masses of the SpC and thymus were greater in the 15-year-old phantoms than those in the adult phantoms. Furthermore, significant differences were observed between S-Ss in the adult (mainly male) and 15-year-old phantoms for the ReW and bronchi as those organs have different masses [17, 18].

The calculated S-Ss and OpenDose data for the ICRP reference adult male and female phantoms were identical, as shown in Fig. 5. This can be attributed to the correlation between the modeling methods. The average ratio for AM and AF was 1.015 from the S-Ss listed in Table 1 and ~~is~~ plotted in Fig. 3. Furthermore, for all the simulated sources, the ratio was approximately 1, which revealed that the DoseCalcs code perfectly reproduced the reference S-S in the voxel-based models.

Fig. 3

^{18}F self-absorption *S*-values (mGy/(MBq s)) for all the simulated source regions in the adult and 15-year-old ICRP models for male and female

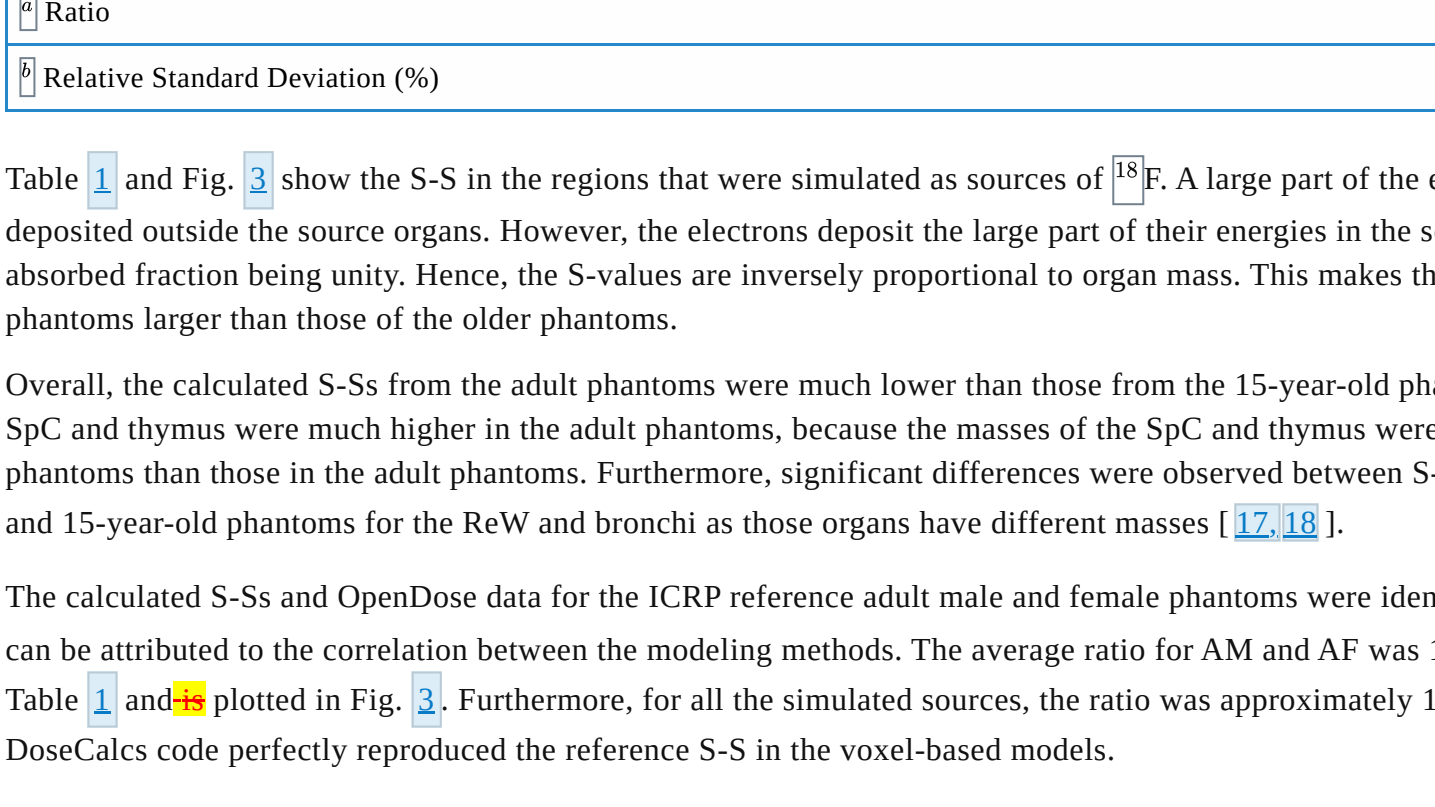

^{18}F cross-irradiation *S*-values (mGy/(MBq s)) for different target←source combinations in the adult and 15-year-old ICRP models for male and female

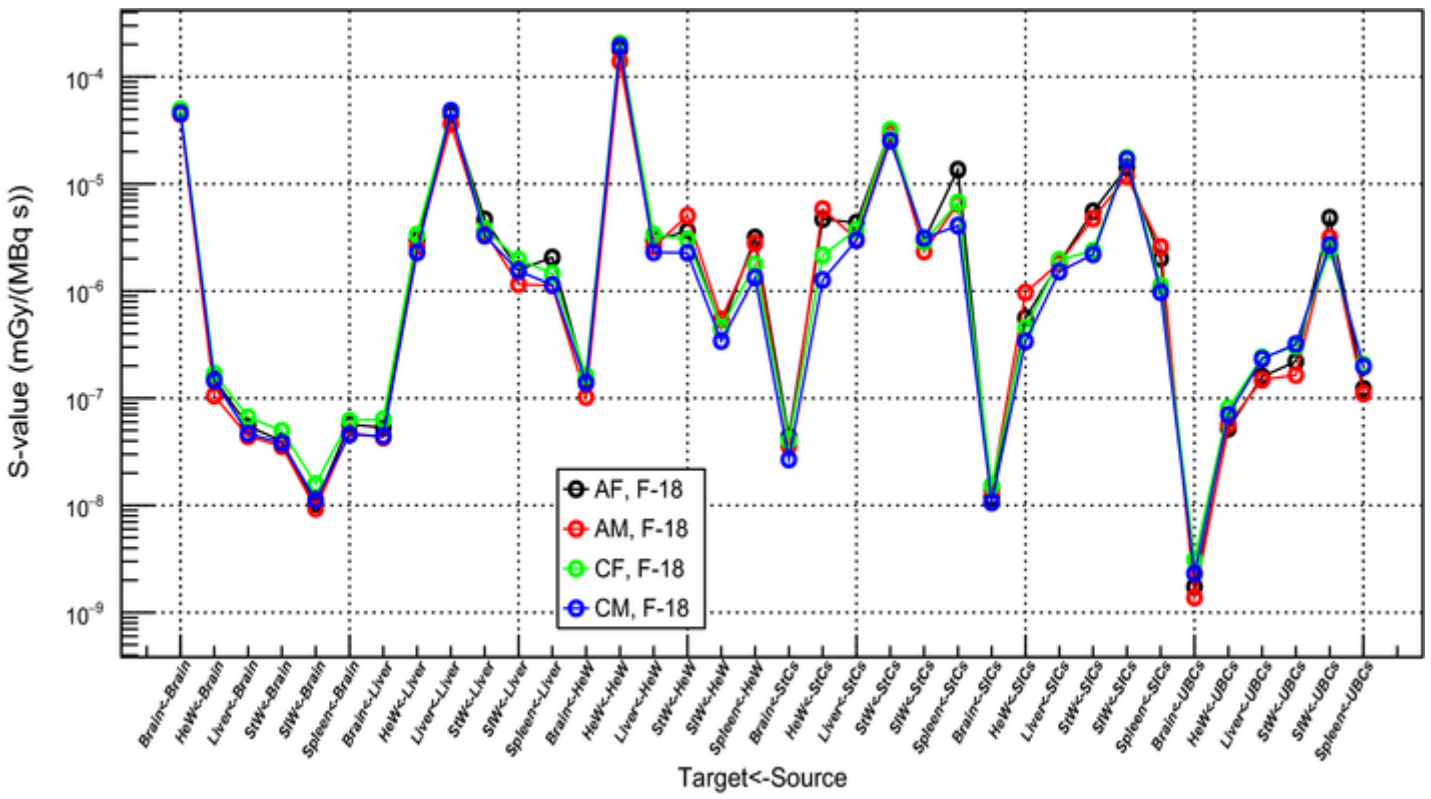

Fig. 5

Ratios between the self-absorption and cross-irradiation S-values of the ICRP adult male and female phantom obtained in this study and to those reported by OpenDose [29]

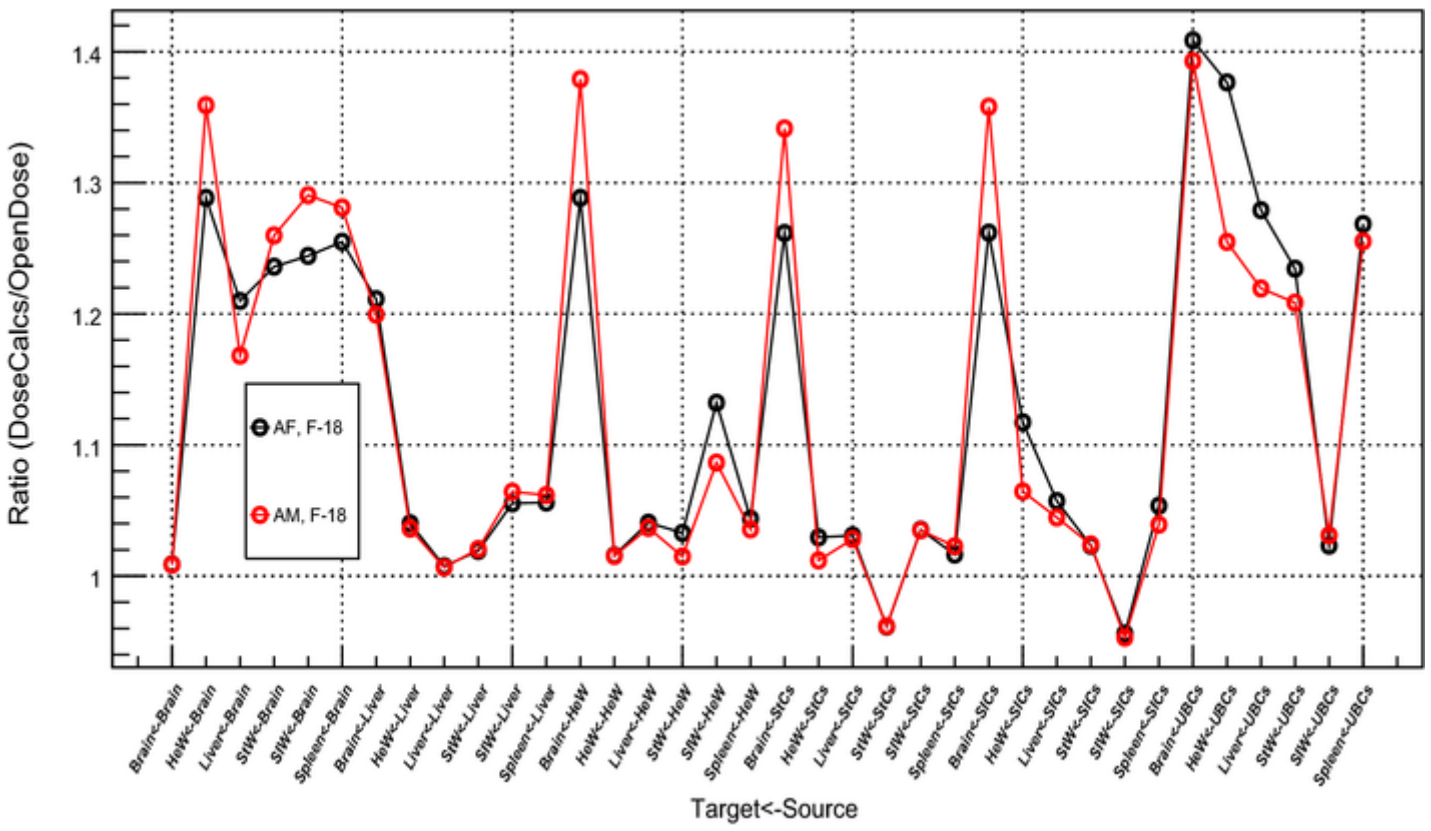

Following the ^{18}F-FDG biokinetic model, Table 2 and Fig. 4 show the C-S from the source regions with high uptake of ^{18}F-FDG, such as the brain, HeW, liver, SICs, StCs, and UBCs [20]. The target regions were the brain, liver, spleen, HeW, SIW, UBW, and StW.

Theoretically, a shorter phantom can provide a shorter distance between the organs, which results in larger C-S ~~-value~~s. In addition, Fig. 4 shows a strong dependence on distance from the source organ. Consequently, organs that are closer to each other receive a higher dose. Most of the *S*-values of the corresponding organs in the 15-year-old phantoms (especially those of female~~s~~) were higher than those in adult~~ss~~ because of the shorter height of the 15-year-old phantom and shorter target←source distances. However, this was not true for all organs. Figure 4 shows that the C-Ss calculated from adult phantoms were overall much lower than 15-year-old phantoms; nevertheless, the C-S in StW←HeW, Spleen←HeW, HeW←StCs, Spleen←SICs, and StW←SICs were much higher for adults. The fraction of emitted energy absorbed from the source region by the target tends to decrease when the inter-organ distance increases in larger phantoms, and the target organ mass increases with the size of the phantom. For instance, the C-S to HeW, StW, and spleen ~~-ratios~~ were higher for adult phantoms owing to the increase in target mass for adults, which compensates for the effect of inter-organ distance. Furthermore, it could originate from the differences in the shapes and locations of organs between the models [17, 18].

Next, we compared the DoseCalcs-obtained C-Ss of the AM and AF models with those from OpenDose [29]. The S-values for 48 combinations are given in Table 2 and the (DoseCalcs/OpenDose) ratios are plotted in Fig. 5. The average ratios for AM and AF were 1.2 and 1.22, respectively. The contribution to the mean ratio was from the distant source–target combinations that included the brain and UBCs as a source or target. The maximum ratios obtained were 1.41 (Brain←UBCs), 1.38 (HeW←UBCs), and 1.34 (UBW←HeW) for AF. Otherwise, the ratios were approximately 1~~one~~ for most of the listed combinations.

DoseCalcs precisely simulated the specific energy of the emitted ^{18}F particles (0.511 MeV for γ and 0.249776 MeV for β) and then calculated the *S*-values. In contrast, for OpenDose values, the complete beta spectrum was simulated, and the electron and photon data energy points were interpolated to estimate the ^{18}F *S*-values. Hence, the macroscopic cross-section of the particle energy was influenced by the distant source–target condition and material heterogeneity across that distance. Because the S-value depends on the macroscopic cross-section, the ratio (DoseCalcs/OpenDose) mainly depends on the calculation method used to estimate the S-values. In addition, the difference in the Monte Carlo codes used could be a possible reason for this.

Figure 6 shows that the S-values calculated in AM for .O were overall higher than .N and .C. In Fig. 7, the ratios show that DoseCalcs and OpenDose S-values have the same tendency and seem to be in good agreement for most combinations, and the mean ratio for all radionuclides was approximately 1.1. Except for StW.StCs whose S-value was lower than OpenDose, and the combinations that included the brain as a source or target, S-values were higher than OpenDose. It is clear that high ratios are registered for .O.

Fig. 6

.C, .N, and .O *S*-values (mGy/(MBq s)) for different target.source combinations in the ICRP adult male model

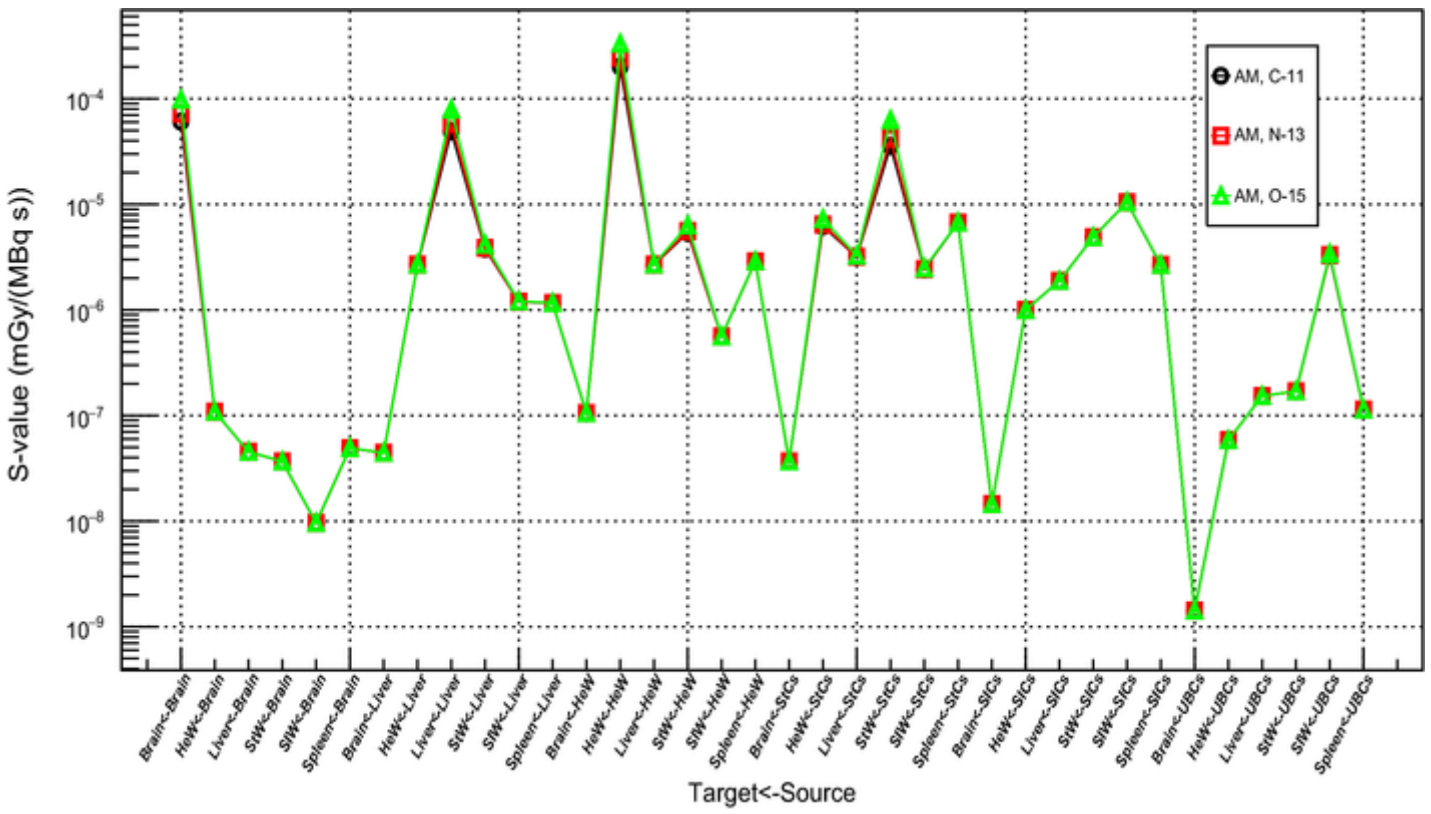

Fig. 7

.C, .N, and .O ratios between *S*-values of the ICRP adult male obtained in this study and those reported by OpenDose [29]

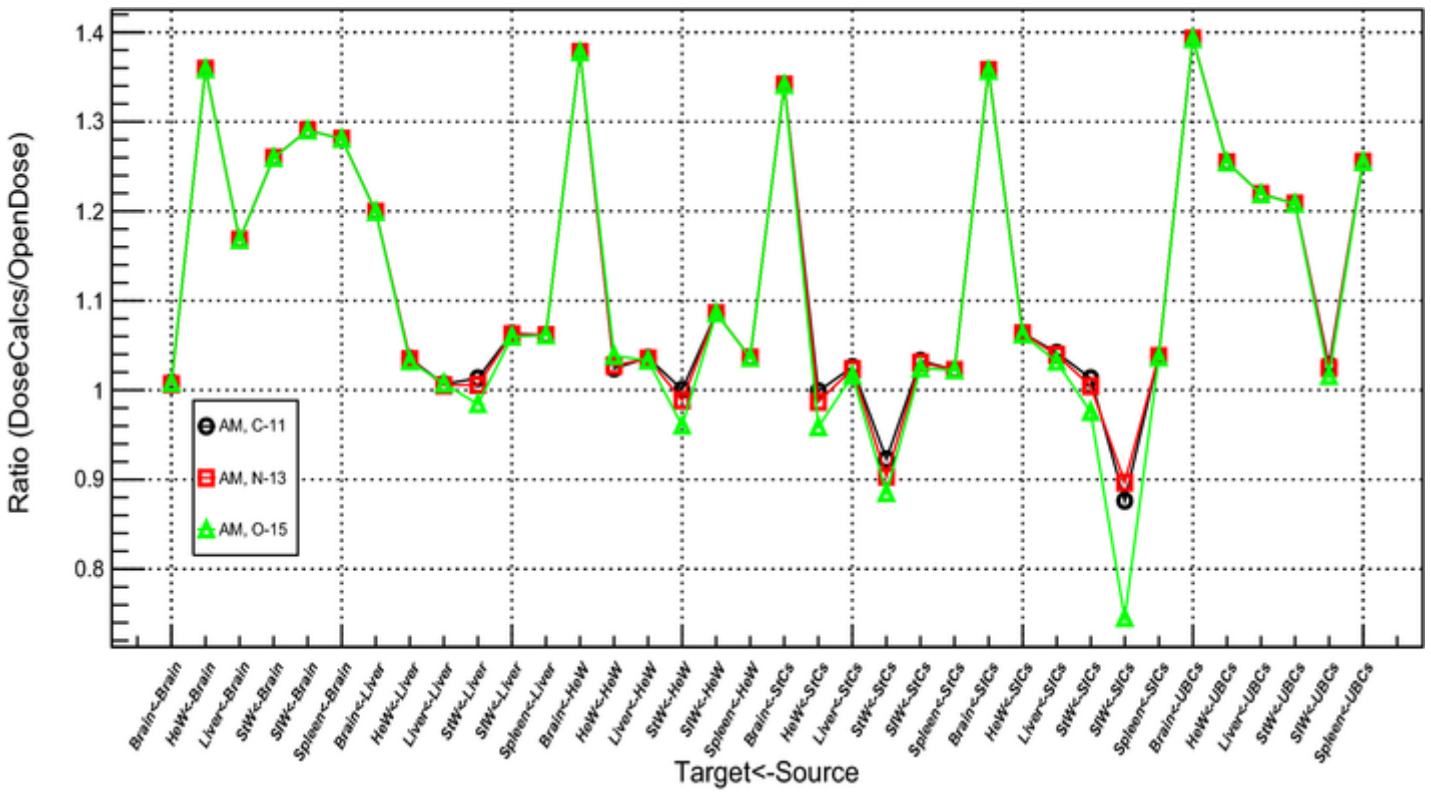

Due to the high energy emitted from .O compared with .N, .C, and .F [19], the calculated S-values in AM for .O were much higher than .N, .C, and .F. As observed for .F, Fig. 6 shows a high dependence of the C-Ss on the distance from the source organ. Consequently, combinations with a large distance between the source and target resulted in lower C-Ss and high ratios. Moreover, when an absorber material fills a large volume between the source and target, the C-Ss will be lower, because the emitted radiation will be absorbed before reaching the target region. The variation in the S-values observed for radionuclides could be attributed primarily to the difference in the calculation technique adopted in this study, which uses . mean energy instead of the full spectrum and the physics applied to transport photons and . particles.

4. Conclusion

This study aimed to validate the DoseCalcs code for calculating the S-values using voxel-based phantoms. We used a previously published set of ICRP computational phantoms representing adult and 15-year-old male and female phantoms to calculate and derive a new set of *S*-values for the ^{18}F radionuclide, which is frequently used in nuclear medicine. We confirmed that the phantoms for 15-year-olds exhibited higher *S*-values than those for older people. The attached file contains the *S*-values calculated in this study for ^{18}F. A comparison of the DoseCalcs results and OpenDose data indicated that the obtained results were consistent with OpenDose under both self-absorption and cross-irradiation conditions. This indicates that the ^{18}F *S*-values can be estimated using the ^{18} mean energy.

The integration of these comprehensive S-values is expected to facilitate absorbed-dose calculations for various phantom regions for patients undergoing ^{18}F nuclear medicine procedures.

Publisher's Note

Springer Nature remains neutral with regard to jurisdictional claims in published maps and institutional affiliations.

Declarations

Conflict of interest The authors declare that they have no conflict of interest.

Human and animal rights statement This study did not involve human participants and animals.

Supplementary Information

Below is the link to the electronic supplementary material.

Supplementary file1 (PDF 706 KB)

Supplementary file2 (CSV 275 KB)

References

1. Ollinger JM, Fessler JA. Positron-emission tomography. Ieee Signal Process Mag. 1997;14(1):43–55.
2. McKeighen RE. A review of gamma camera technology for medical imaging. Nuclear Med Ultrasonics Thermogr. 1980; chap. 4, p. 119–63.
3. Huang B, Law MW-M, Khong P-L. Whole-body PET/CT scanning: estimation of radiation dose and cancer risk. Radiology. 2009;251:166–74.
4. Glatting G, Lassmann M. Nuclear medicine dosimetry: quantitative imaging and dose calculations. Z Med Phys. Dec.2011;21:246–7.
5. Endo M. History of medical physics. Radiol Phys Technol. Dec.2021;14:345–57.
6. Alauddin MM. Positron emission tomography (pet) imaging with 18f-based radiotracers. Am J Nucl Med Mol imaging. 2012;2(1):55.
7. Duhaylongsod FG, Lowe VJ, Patz EF Jr, Vaughn AL, Coleman RE, Wolfe WG. Detection of primary and recurrent lung cancer by means of f-18 fluorodeoxyglucose positron emission tomography (fdg pet). J Thorac Cardiovasc Surg. 1995;110(1):130–40.
8. Spermon J, De Geus-Oei L, Kiemeney L, Witjes J, Oyen W. The role of 18fluoro-2-deoxyglucose positron emission tomography in initial staging and re-staging after chemotherapy for testicular germ cell tumours. BJU Int. 2002;89(6):549–56.
9. Sodickson L, Bowman W, Stephenson J, Weinstein R. Single-quantum annihilation of positrons. Phys Rev. 1961;124(6):1851.
10. Ter-Pogossian MM, Phelps ME, Hoffman EJ, Mullani NA. A positron-emission transaxial tomograph for nuclear imaging (pett). Radiology. 1975;114(1):89–98.
11. Partridge S, Timothy A, O'doherty M, Hain S, Rankin S, Mikhaeel G. T2-fluorine-18-fluoro-2-deoxy-d glucose positron emission tomography in the pretreatment staging of Hodgkin's disease: influence on patient management in a single institution. Ann Oncol. 2000;11(10):1273–80.
12. Ahmadi N, Karimian A, Nasrabadi M, Rahmim A. Assessment of fetal and maternal radiation absorbed dose in 18f-fdg pet imaging. Int J Radiat Res. 2019;17(4):651–7.
13. Dunn WL, Shultis JK. Exploring Monte Carlo methods. Elsevier; 2011.

14. Shi C, Xu XG, Stabin MG. Saf values for internal photon emitters calculated for the rpi-p pregnant-female models using Monte Carlo methods. Med Phys. 2008;35(7Part1):3215–24.

15. Caon M. Voxel-based computational models of real human anatomy: a review. Radiat Environ Biophys. Feb.2004;42:229–35.

16. Kim KM, Lee MS, Suh MS, Selvam HSMS, Tan TH, Cheon GJ, Kang KW, Lee JS. Comparison of voxel s-value methods for persona lized voxel-based dosimetry of 177lu-dotatate. Med Phys. 2022;49(3):1888–901.

17. Zankl M. Adult male and female reference computational phantoms (ICRP publication 110). Jpn J Health Phys. 2010;45(4):357–69.

18. Bolch WE, Eckerman K, Endo A, Hunt JGS, Jokisch DW, Kim CH, Kim K-P, Lee C, Li J, Petoussi-Henss N, Sato T, Schlattl H, Yeom YS, Zankl M. ICRP publication 143: paediatric reference computational phantoms. Ann ICRP. 2020;49:5–297.

19. Eckerman K, Endo A. ICRP publication 107. nuclear decay data for dosimetric calculations. Ann ICRP. 2008;38(3):7–96.

20. Mattsson S, Johansson L, Leide Svegborn S, Liniecki J, Noßke D, Riklund KÅ, Stabin M, Taylor D, Bolch W, Carlsson S, Eckerman K, Giussani A, Söderberg L, Valind S, ICRP. Radiation dose to patients from radiopharmaceuticals: a compendium of current informat ion related to frequently used substances. Ann ICRP. 2015;44:7–321.

21. Stabin MG. Mirdose: personal computer software for internal dose assessment in nuclear medicine. J Nucl Med. 1996;37(3):538–46.

22. Stabin MG, Sparks RB, Crowe E. Olinda/exm: the second-generation personal computer software for internal dose assessment in nucl ear medicine. J Nucl Med. 2005;46(6):1023–7.

23. Werner CJ, Bull JS, Solomon CJ, Brown FB, McKinney GW, Rising ME, Dixon DA, Martz RL, Hughes HG, Cox LJ, Zukaitis AJ, Ar mstrong JC, Forster RA, Casswell L. MCNP version 6.2 release notes. Tech. Rep., 2018.

24. Agostinelli S, Allison J, Amako K, Apostolakis J, Araujo H, Arce P, Asai M, Axen D, Banerjee S, Barrand G, Behner F, Bellagamba L, Boudreau J, Broglia L, Brunengo A, Burkhardt H, Chauvie S, Chuma J, Chytracek R, Cooperman G, Cosmo G, Degtyarenko P, Del l'Acqua A, Depaola G, Dietrich D, Enami R, Feliciello A, Ferguson C, Fesefeldt H, Folger G, Foppiano F, Forti A, Garelli S, Giani S, Giannitrapani R, Gibin D, Gómez Cadenas JJ, González I, Gracia Abril G, Greeniaus G, Greiner W, Grichine V, Grossheim A, Guatell i S, Gumplinger P, Hamatsu R, Hashimoto K, Hasui H, Heikkinen A, Howard A, Ivanchenko V, Johnson A, Jones FW, Kallenbach J, Kanaya N, Kawabata M, Kawabata Y, Kawaguti M, Kelner S, Kent P, Kimura A, Kodama T, Kokoulin R, Kossov M, Kurashige H, La manna E, Lampén T, Lara V, Lefebure V, Lei F, Liendl M, Lockman W, Longo F, Magni S, Maire M, Medernach E, Minamimoto K, Mora de Freitas P, Morita Y, Murakami K, Nagamatu M, Nartallo R, Nieminen P, Nishimura T, Ohtsubo K, Okamura M, O'Neale S, Oohata Y, Paech K, Perl J, Pfeiffer A, Pia MG, Ranjard F, Rybin A, Sadilov S, Di Salvo E, Santin G, Sasaki T, Savvas N, Sawada Y, S cherer S, Sei S, Sirotenko V, Smith D, Starkov N, Stoecker H, Sulkimo J, Takahata M, Tanaka S, Tcherniaev E, Safai Tehrani E, Trope ano M, Truscott P, Uno H, Urban L, Urban P, Verderi M, Walkden A, Wander W, Weber H, Wellisch JP, Wenaus T, Williams DC, Wrig ht D, Yamada T, Yoshida H, Zschiesche D. Geant4–a simulation toolkit. Nucl Instrum Methods Phys Res A. 2003;506:250–303.

25. Jan S, Santin G, Strul D, Staelens S, Assié K, Autret D, Avner S, Barbier R, Bardiès M, Bloomfield PM, Brasse D, Breton V, Bruyndo nckx P, Buvat I, Chatziioannou AF, Choi Y, Chung YH, Comtat C, Donnarieix D, Ferrer L, Glick SJ, Groiselle CJ, Guez D, Honore P F, Kerhoas-Cavata S, Kirov AS, Kohli V, Koole M, Krieguer M, van der Laan DJ, Lamare F, Largeron G, Lartizien C, Lazaro D, Maas MC, Maigne L, Mayet F, Melot F, Merheb C, Pennacchio E, Perez J, Pietrzyk U, Rannou FR, Rey M, Schaart DR, Schmidtlein CR, Si mon L, Song TY, Vieira JM, Visvikis D, Van de Walle R, Wieërs E, Morel C. GATE: a simulation toolkit for PET and SPECT. Phys M ed Biol. 2004;49:4543–61.

26. Stabin MG, Xu XG, Emmons MA, Segars WP, Shi C, Fernald MJ. Radar reference adult, pediatric, and pregnant female phantom seri es for internal and external dosimetry. J Nucl Med. 2012;53(11):1807–13.

27. Ghalbzouri TE, Bardouni TE, Bakkali JE, Satti H, Arectout A, Berriban I, Nouayti A, Yerrou R. Photon-specific absorbed fraction esti mates in stylized ORNL and voxelized ICRP adult male phantoms using a new developed geant4-based code "DoseCalcs": a validatio n study. Radiol Phys Technol. 2022. https://dosecalcs.readthedocs.io/en/latest/index.html.

28. Parach AA, Rajabi H, Askari MA. Assessment of MIRD data for internal dosimetry using the GATE Monte Carlo code. Radiat Enviro n Biophys. 2011;50:441–50.

29. Chauvin M, Borys D, Botta F, Bzowski P, Dabin J, Denis-Bacelar AM, Desbrée A, Falzone N, Lee BQ, Mairani A, Malaroda A, Mathi eu G, McKay E, Mora-Ramirez E, Robinson AP, Sarrut D, Struelens L, Gil AV, Bardiès M. OpenDose: open-access resource for nucle ar medicine dosimetry. J Nucl Med. 2020;61:1514–9.

I, Rogers D. The egsnrc code system. NRC Report PIRS-701, NRC, Ottawa, vol. 17, 2000.

31. Böhlen T, Cerutti F, Chin M, Fassò A, Ferrari A, Ortega PG, Mairani A, Sala PR, Smirnov G, Vlachoudis V. The fluka code: developments and challenges for high energy and medical applications. Nucl Data Sheets. 2014;120:211–4.

32. Allison J, Amako K, Apostolakis J, Arce P, Asai M, Aso T, Bagli E, Bagulya A, Banerjee S, Barrand G, et al. Recent developments in geant4. Nucl Instrum Methods Phys Res Sect A. 2016;835:186–225.

33. Salvat F, Fernández-Varea JM, Sempau J, et al. Penelope-2008: A code system for Monte Carlo simulation of electron and photon transport. In: Workshop Proceedings, Barcelona. Spain. 2008;30.

34. Chytracek R, Mccormick J, Pokorski W, Santin G. Geometry description markup language for physics simulation and analysis applications. IEEE Trans Nucl Sci. 2006;53:2892–6.

35. Stroud I, Xirouchakis PC. STL and extensions. Adv Eng Softw. 2000;31:83–95.

36. Group G. TEXT file geometry manual, 2009.

37. Snir M, Gropp W, Otto S, Huss-Lederman S, Dongarra J, Walker D. MPI-the Complete Reference: the MPI core. 1998;1

38. Ahn S, Apostolakis J, Asai M, Brandt D, Cooperman G, Cosmo G, Dotti A, Dong X, Yung Jun S, Nowak A. GEANT4-MT : bringing multi-threading into GEANT4 production. In: Caruge D, Calvin C, Diop CM, Malvagi F, J.-C. Trama J-C. editors. SNA + MC 2013 - Joint International Conference on Supercomputing in Nuclear Applications + Monte Carlo, (Les Ulis, France), EDP Sciences, 2014.

39. Brun R, Rademakers F. ROOT—an object oriented data analysis framework. Nucl Instrum Methods Phys Res A. 1997;389:81–6.

40. Bolch WE, Eckerman KF, Sgouros G, Thomas SR. MIRD pamphlet no. 21: a generalized schema for radiopharmaceutical dosimetry-standardization of nomenclature. J Nucl Med. 2009;50:477–84.

41. Dias AH, Hansen AK, Munk OL, Gormsen LC. Normal values for 18F-FDG uptake in organs and tissues measured by dynamic whole body multiparametric FDG PET in 126 patients. EJNMMI Res. 2022;12:15.

42. Arce P, Bolst D, Bordage M-C, Brown JMC, Cirrone P, Cortés-Giraldo MA, Cutajar D, Cuttone G, Desorgher L, Dondero P, Dotti A, Faddegon B, Fedon C, Guatelli S, Incerti S, Ivanchenko V, Konstantinov D, Kyriakou I, Latyshev G, Le A, Mancini-Terracciano C, Maire M, Mantero A, Novak M, Omachi C, Pandola L, Perales A, Perrot Y, Petringa G, Quesada JM, Ramos-Méndez J, Romano F, Rosenfeld AB, Sarmiento LG, Sakata D, Sasaki T, Sechopoulos I, Simpson EC, Toshito T, Wright DH. Report on G4-Med, a geant4 benchmarking system for medical physics applications developed by the geant4 medical simulation benchmarking group. Med Phys. 2021;48:19–56.